

Testing Computational Algorithms for Unsaturated Flow

F.T. Tracy*

Department of Defense (DoD) Supercomputing Resource Center (DSRC), Information Technology Laboratory (ITL), Engineer Research and Development Center (ERDC), Vicksburg, MS, USA

Abstract: The purpose of this work is to test different computational algorithms for unsaturated flow for accuracy and robustness by comparing computed results in a finite element program with analytical solutions. Because real-world problems are complex, testing codes for accuracy is often difficult. This is particularly true for flow in the vadose zone where Richards' equation is highly nonlinear. Recently, however, Tracy (Tracy WRRJ 2006) [1] (Tracy JHYD 2007) [2] has derived analytical solutions for a box-shaped flow region that is initially dry until water is applied to the top of the region. Two-dimensional and three-dimensional versions of these solutions for both steady-state and transient flow are available to be used in the testing process. Numerical precision and nonlinear solver robustness were investigated for varying degrees of nonlinearity by varying the Gardner α parameter. As α was increased, three ways of modeling relative hydraulic conductivity inside individual finite elements and two versions of the nonlinear solver were tested using three different ways to measure the error. The results of these tests are given in this paper.

Keywords: Unsaturated flow, finite element method, nonlinear system of equations, Newton and Picard linearizations, Richards' equation.

1. INTRODUCTION

Because real-world problems are complex, testing unsaturated groundwater simulation finite element (FE) codes for accuracy is often difficult. This is particularly true when part or all of the flow is in the vadose zone where Richards' equation is highly nonlinear. Recently, analytical solutions have been derived (Tracy WRRJ 2006) [1] (Tracy JHYD 2007) [2] for a box-shaped flow region that is initially dry until water is applied to the top of the region. Two-dimensional (2-D) and three-dimensional versions of these solutions for both steady-state and transient flow are available, and one of the 2-D solutions was used in this study as a test problem. Another excellent feature of this test problem is that its nonlinearity can be reduced or increased by changing the Gardner parameter, α . As shown in more detail in Section 2 describing Richards' equation, this conservation of water partial differential equation (PDE) for total head has coefficients in it (such as relative hydraulic conductivity) that are functions of pressure head, too, thus creating a nonlinear PDE. During saturated flow, relative hydraulic conductivity is equal to one, and the steady-state flow equation in a homogeneous, isotropic, incompressible medium becomes the linear partial differential equation of Laplace's equation.

Another challenge in the FE program is that the nonlinear solver has trouble converging when the nonlinearity of the problem is significant. The ideal algorithm is one that is robust and accurate. The goal of this study is to determine the impact on accuracy and robustness in an unsaturated FE

flow simulation code when increasing the nonlinearity of the test problem. It is hoped that from this research, clear recommendations can be provided for real-world FE simulations. Specifically, as α is increased, the following were considered for the transient problem: (1) three ways to model relative hydraulic conductivity inside individual finite elements, and (2) two versions of the nonlinear solver. Three error metrics were used for each test. A smaller study was done for the steady-state case.

2. RICHARDS' EQUATION

The general version of Richards' equation for unsaturated flow that is used in this work has the following form:

$$\nabla \cdot (k_r K_s \cdot \nabla \phi) = \frac{\partial \theta}{\partial t} \quad (1)$$

with the definition,

$$\phi = h + z \quad (2)$$

where k_r is the relative hydraulic conductivity, K_s is the saturated hydraulic conductivity tensor, ϕ is the total head, θ is the moisture content, t is the time, h is the pressure head, and z is the vertical co-ordinate. The form used in the FE program is

$$k_s \nabla \cdot (k_r \nabla \phi) = \frac{d\theta}{dh} \frac{\partial \phi}{\partial t} = w_c \frac{\partial \phi}{\partial t} \quad (3)$$

where w_c is the water capacity, and k_s is the scalar isotropic, homogeneous saturated hydraulic conductivity. The version of Richards' equation that is the foundation for deriving the analytical solution used for the test problem is

$$\nabla \cdot (k_r \cdot \nabla h) + \frac{\partial k_r}{\partial z} = \frac{1}{k_s} \frac{\partial \theta}{\partial t} \quad (4)$$

*Address correspondence to this author at the Department of Defense (DoD) Supercomputing Resource Center (DSRC), Information Technology Laboratory (ITL), Engineer Research and Development Center (ERDC), Vicksburg, MS, USA; Tel: (601) 634-4112; Fax: (601) 634-2324; E-mail: Fred.T.Tracy@usace.army.mil

2.1. Relative Hydraulic Conductivity

Relative hydraulic conductivity is modeled by the quasi-linear assumption (Gardner SS 1958) [3],

$$k_r = e^{\alpha h} \tag{5}$$

This can be compared with the more well-known van Genuchten equation (van Genuchten SSAJ 1980) [4],

$$k_r = \frac{\left\{ 1 - (-\xi h)^{\rho-1} \left[1 + (-\xi h)^\rho \right]^{-\mu} \right\}^2}{\left[1 + (-\xi h)^\rho \right]^{\mu/2}} \tag{6}$$

with

$$\mu = 1 - \frac{1}{\rho} \tag{7}$$

where ξ , ρ , and μ are parameters. Fig. (1) shows a sample comparison of the two methods with $\xi = 0.17 \text{ cm}^{-1}$, $\rho = 2$, $\mu = 1/2$, and $\alpha = 0.45 \text{ cm}^{-1}$. The same characteristic steep descent is achieved in either equation. However, it must be cautioned that matching Gardner and van Genuchten curves is not always successful (Rucker, Warrick, and Ferré AWRJ 2005) [5]. The justification for using the Gardner approximation for relative hydraulic conductivity instead of the van Genuchten curve is not how well these curves can be matched; rather, it is that the Gardner approximation is needed to derive the analytical solution used as the test problem. Fig. (2) shows a plot of (5) for three different values of α .

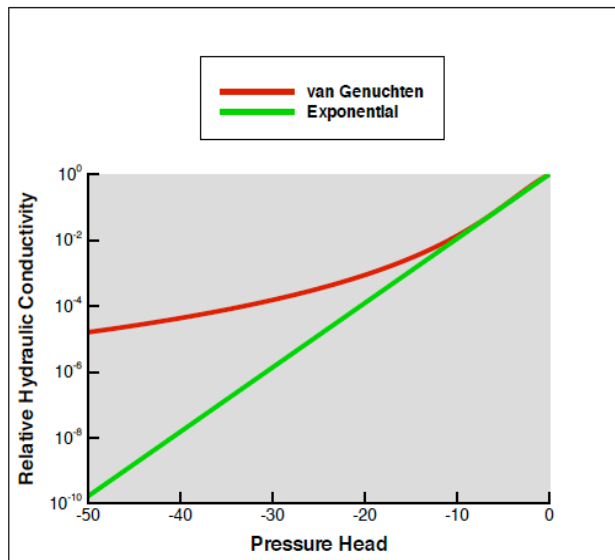


Fig. (1). Plot of relative hydraulic conductivity versus pressure head for the exponential and van Genuchten equations for $\xi = 0.17 \text{ cm}^{-1}$, $\mu = 1/2$, $\rho = 2$, and $\alpha = 0.45 \text{ cm}^{-1}$.

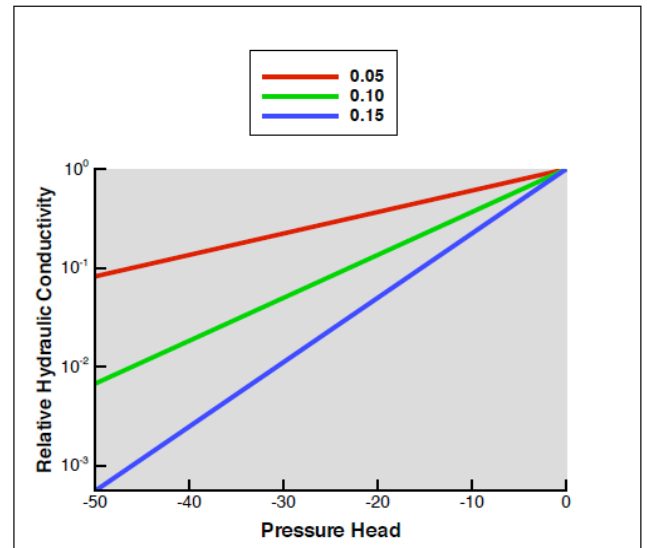


Fig. (2). Plot of relative hydraulic conductivity versus pressure head for $\alpha = 0.05, 0.10, \text{ and } 0.15 \text{ cm}^{-1}$.

2.2. Moisture Content

Moisture content, θ , is computed from a linear variation between θ and k_r (Irmay ETAGU 1954) [6]. What is used is

$$\theta = (\theta_s - \theta_d)k_r + \theta_d \tag{8}$$

where θ_s is the saturated moisture content, and θ_d is the moisture content when the soil is dry.

3. FINITE ELEMENT FORMULATION

The FE procedure discussed here starts with (3) and uses a standard continuous Galerkin fully implicit approach (Istok AGU 1989) [7], (Cook John Wiley & Sons 1981) [9] using the linear, triangular isoparametric element to produce for a given finite element,

$$A_e k_{se} (k_r)_e^{n+1} B^T B \varphi_e^{n+1} + \frac{A_e}{3\Delta t} \begin{bmatrix} w_{c1} & 0 & 0 \\ 0 & w_{c2} & 0 \\ 0 & 0 & w_{c3} \end{bmatrix} (\varphi_e^{n+1} - \varphi_e^n) = Q_e \tag{9}$$

where A_e is the area of an element; k_{se} is the saturated hydraulic conductivity of an element; Δt is the time-step size; $(k_r)_e^{n+1}$ is the equivalent constant relative hydraulic conductivity of an element (see Section 3.1) at time-step, $n+1$, of an element; B is a 2×3 matrix that depends only on the geometry of an element; φ_e^{n+1} is the vector of total head for the three nodes of an element at time-step, $n+1$; w_{c1} is water capacity of the first node of an element; w_{c2} is water capacity of the second node of an element; w_{c3} is water capacity of the third node of an element; and Q_e is a vector of known flow-type terms for the three nodes of an element. $(k_r)_e$ is given by

$$(k_r)_e = \frac{1}{A_e} \int_{A_e} k_r(h(x,z)) dA \quad (10)$$

B comes from the gradient of the transpose of the vector of local interpolation functions, L . ϕ , x , and z are interpolated by

$$\begin{aligned} \phi &= L^T \varphi_e^{n+1} \\ x &= L^T X_e \\ z &= L^T Z_e \end{aligned} \quad (11)$$

$$\sum_{i=1}^3 (L)_i = 1$$

inside individual finite elements. Here, (X_e, Z_e) are vectors of the (x, z) coordinates of the three nodes of a triangular element, and $(L)_i$ is the i^{th} interpolation function. This notation for $(L)_i$ as used in (Kelley SIAM 2003) [8] for the i^{th} component of a vector will be used throughout this paper. From common FE derivation, B is

$$B = \nabla L^T \quad (12)$$

Using (11), B can then be computed. It is important to note that the time term is treated as the "lumped mass" scheme.

3.1. Relative Hydraulic Conductivity Models

Discussion has risen at times about how to numerically handle the relative hydraulic conductivity in finite element programs. Three ways of modeling relative hydraulic conductivity inside a 2-D triangular finite element were considered, and they are as follows:

1. Constant k_r in the element using a simple average of pressure head of the nodes of an element.

$$\bar{h}_e = \frac{1}{3} \sum_{j=1}^3 h_j \quad (13)$$

$$(k_r)_e = k_r(\bar{h}_e) \quad (14)$$

2. Linearly varying k_r over the element. This is equivalent to

$$(k_r)_e = \frac{1}{3} \sum_{j=1}^3 k_r(h_j) \quad (15)$$

3. Numerically integrating k_r over the element. From the definition,

$$\begin{Bmatrix} \hat{h}_1 \\ \hat{h}_2 \\ \hat{h}_3 \end{Bmatrix} = \frac{1}{6} \begin{bmatrix} 4 & 1 & 1 \\ 1 & 4 & 1 \\ 1 & 1 & 4 \end{bmatrix} \begin{Bmatrix} h_1 \\ h_2 \\ h_3 \end{Bmatrix} \quad (16)$$

this case is equivalent to

$$(k_r)_e = \frac{1}{3} \sum_{j=1}^3 k_r(\hat{h}_j) \quad (17)$$

4. NONLINEAR SOLVER

The FE program uses either a full exact Newton nonlinear iteration (Kelley SIAM 2003) [8] or a Picard nonlinear iteration (Putti and Paniconi CMWR 1992) [10] applied to (9) at any given nonlinear iteration. To test the robustness of the nonlinear solution, various numbers of Picard iterations were sometimes used before the full Newton solver was turned on. In all cases, a bisection line search was used at each nonlinear iteration. Nonlinear convergence was achieved when the maximum change in total head at any node was less in magnitude than 10^{-5} when comparing the current nonlinear iteration to the previous one.

5. TEST PROBLEM

The test problem consists of applying water to the top of a vertical 2-D cross-section of soil with dimensions, $a \times L$, that is initially dry (see Fig. 3).

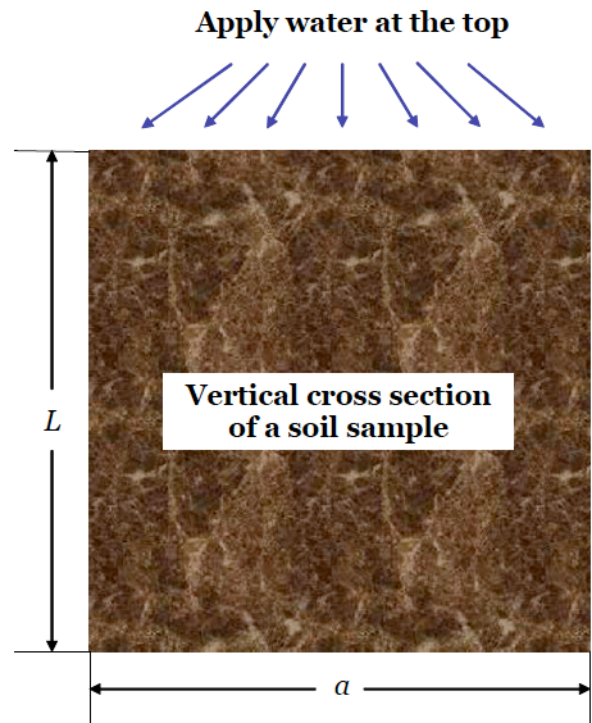


Fig. (3). Plot of the test problem showing a vertical cross-section of soil with dimensions, $a \times L$, and water being applied at the top.

5.1. Initial and Boundary Conditions

The initial condition at time, $t = 0$, for $0 \leq x \leq a, 0 \leq z \leq L$ is

$$h(x, z, 0) = h_d \quad (18)$$

where h_d is the pressure head when the soil is dry. Starting with the definition,

$$\varepsilon_d = e^{c h_d} \quad (19)$$

the boundary conditions for $t > 0$ are

$$h(0, z, t) = h(a, z, t) = h(x, 0, t) = h_d \quad (20)$$

$$h(x, L, t) = \frac{1}{\alpha} \ln \left[\varepsilon_d + (1 - \varepsilon_d) \sin \frac{\pi x}{a} \right]$$

where α is a parameter such that the larger it is, the more nonlinear the problem is. Fig. (4) shows a plot of (20) at $z=L$. It is important to note that as α is increased, the absolute values of the respective slopes near $x=0$ and $x=L$ become steeper. This adds further stress in the ability of computer models to be able to solve this test problem.

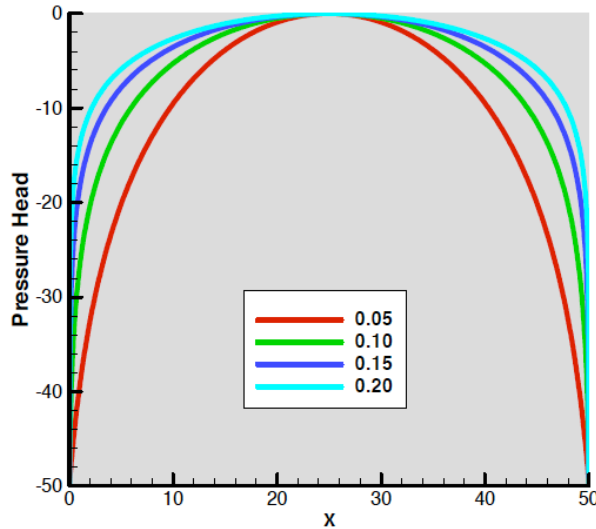


Fig. (4). Plot of the pressure head boundary condition on the top of the soil sample for four values of $\alpha(\text{cm}^{-1})$.

6. RESULTS AND ANALYSIS

Results for the test problem were obtained using the FE program and then compared with the analytical solution (Tracy WRRJ 2006) [1]. The following data were used: $a=L=25$ cm with grid = 101×101 , $a=L=50$ cm with grid = 201×201 , and $a=L=75$ cm with grid = 301×301 ; $k_s = 0.1$ cm/day; $\theta_d = 0.15$; $\theta_s = 0.45$; constant grid spacing = $\Delta x = \Delta z = 0.25$ cm; time-step size = 0.1, 0.01, and 0.001 day; $\alpha = 0.05, 0.10, 0.15$, and 0.20 cm^{-1} ; and a time period of 0.5 and 2.0 day. Each grid square is divided into two triangular finite elements in this work.

Absolute or actual error is used in the reporting of results in this work as compared to relative error. Given a particular computer run, the error at each node is

$$(E)_i = (\varphi)_i - (\Phi)_i, 1 \leq i \leq N \quad (21)$$

where E is the vector of error at the nodes; φ is the vector of total head at the nodes computed by the FE program, Φ is the vector of total head at the nodes computed from the analytical solution, and N is the total number of nodes. Define w as the $(E)_i$ with the largest magnitude or "worst" error among all the nodes. It is important to note that the sign of this worst error is kept. The bias (b) and root-mean-squared error (E_{RMS}) over all the nodes of the grid are given by

$$b = \frac{1}{N} \sum_{i=1}^N (E)_i \quad (22)$$

$$E_{RMS} = \sqrt{\frac{1}{N} \sum_{i=1}^N (E)_i^2} \quad (23)$$

6.1. Accuracy of Computations

Fig. 5(a) shows a plot of the analytical solution of total head for the upper, right-hand corner of the flow region for $\alpha = 0.2 \text{ cm}^{-1}$, $\Delta t = 0.001$ day, and total time = 0.5 day, and Fig. 5(b) - 5(d) show contour plots of E for the three ways of modeling k_r . Figs. (6-17) give plots of worst error, bias error, and RMS error for different values of α , domain size, time duration, and handling of k_r options. Observations are as follows:

1. The plots in Fig. (5) show that the constant k_r model performed the best among the three choices in the middle of the domain with numerically integrated k_r coming in second, and linear k_r coming in last. This is counter-intuitive. A full explanation requires further research, but it is somewhat equivalent to the research that has been done with consistent versus "lumped mass" element matrices for the time term. Sometimes the lumped mass approach (similar to a finite volume approach) does better than the consistent mass formulation, although it is less accurate in the element matrix formulation sense. This appears to also sometimes be true in some sense for the evaluation of the stiffness matrix.

2. The corner effects near the top of the flow region as shown in Fig. (5) are worst in the constant k_r case and best in the numerically integrated k_r case. These corner effects are the result of the steep slope at the corners of the applied boundary condition. Here, it makes perfect sense that the numerically integrated case would do best. This test problem thus becomes an excellent example of where adaptive mesh refinement could be effectively applied, and thus a good option for further research.

3. When looking at the data in Figs. (6-17), linearly varying k_r often does best. Therefore, no one method consistently beats the other. However, the numerically integrated option is recommended more as the nonlinearity increases.

4. As the size of the mesh became bigger, the errors became smaller.

5. As the time period grew longer, the errors became smaller.

6. As the nonlinearity increases, the errors increase.

7. As the nonlinearity increases, the Δt required to get the same accuracy as a less nonlinear problem decreases.

8. Sometimes the errors are positive, and sometimes they are negative. This means that the speed of the moving front of water is not matched exactly by the numerics, and it is sometimes slower and sometimes faster than the actual speed.

6.2. Robustness of Nonlinear Solver

Both the Newton and Picard nonlinear solvers and combinations of the two were tried on the test problem, and Table 1 gives the results. What is given is the nonlinear solver iteration count for various values of α and Δt for the

Table 1. Nonlinear Solver Iteration Count for Various Values of α and Δt for the 201×201 Grid for the First Nonlinear Iteration of the First Time-Step for The Three Relative Hydraulic Conductivity Models for Four Options of the Nonlinear Solver

Nonlinear Solver Type	Δt	α	Constant k_r	Linear k_r	Numerically Integrated k_r
Newton only	0.1	0.05	30	26	14
10 Picard + Newton	0.1	0.05	17	18	14
Picard only	0.1	0.05	14	14	14
Newton only	0.1	0.2	>100	Blew up	27
10 Picard + Newton	0.1	0.2	Blew up	33	27
20 Picard + Newton	0.1	0.2	38	36	27
Picard only	0.1	0.2	32	36	27
Newton only	0.001	0.2	>100	53	20
10 Picard + Newton	0.001	0.2	71	56	20
20 Picard + Newton	0.001	0.2	19	54	20
Picard only	0.001	0.2	19	46	20

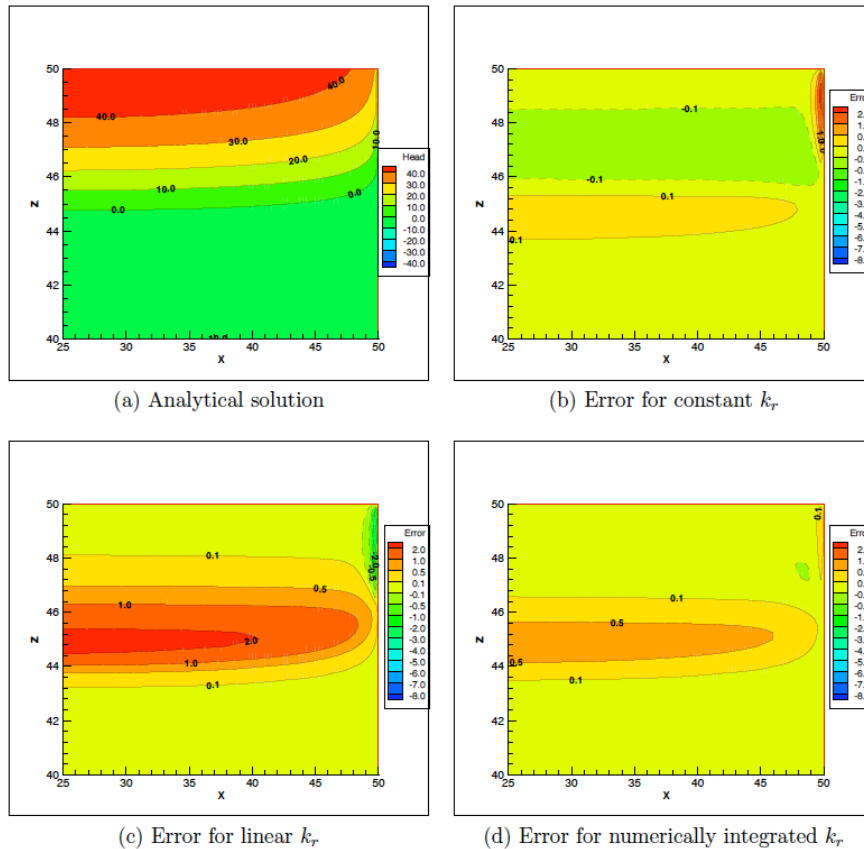


Fig. (5). Plot of the transient analytical solution and error (E) in total head (cm) for the three ways of modeling k_r for the upper, right-hand corner of the flow region for $\alpha = 0.2 \text{ cm}^{-1}$, $\Delta t = 0.001$ day, and total time = 0.5 day.

201×201 grid for the first nonlinear iteration of the first time-step for the three relative hydraulic conductivity models for the four options of only Newton iterations, only Picard iterations, 10 Picard iterations with the remaining nonlinear

iterations being the Newton type, and 20 Picard iterations with the remaining nonlinear iterations being the Newton type. For $\alpha = 0.05 \text{ cm}^{-1}$, all nonlinear solver options worked, and the Newton only option had the fewest iterations.

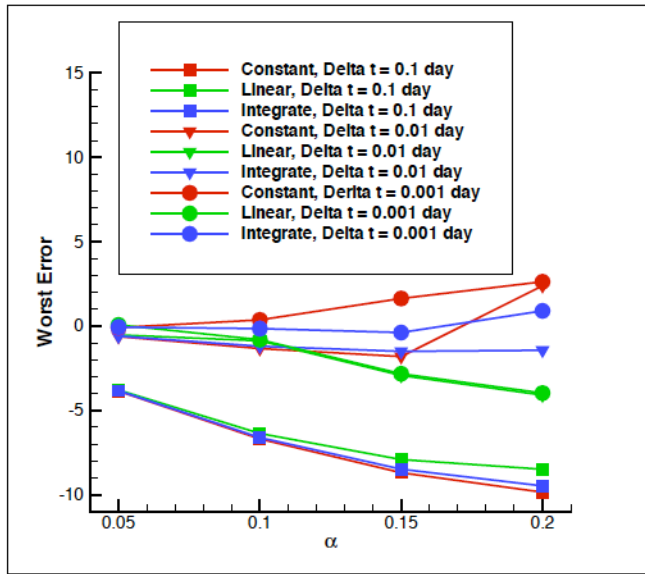


Fig. (6). Plot of worst error (w) of total head (cm) for $\Delta t = 0.1, 0.01,$ and 0.001 day; $L = \alpha = 25$ cm; and $\alpha = 0.05, 0.10, 0.15,$ and 0.2 cm^{-1} after a time period of 0.5 day for the three relative hydraulic conductivity models of constant (C), linear (L), and numerically integrated (I).

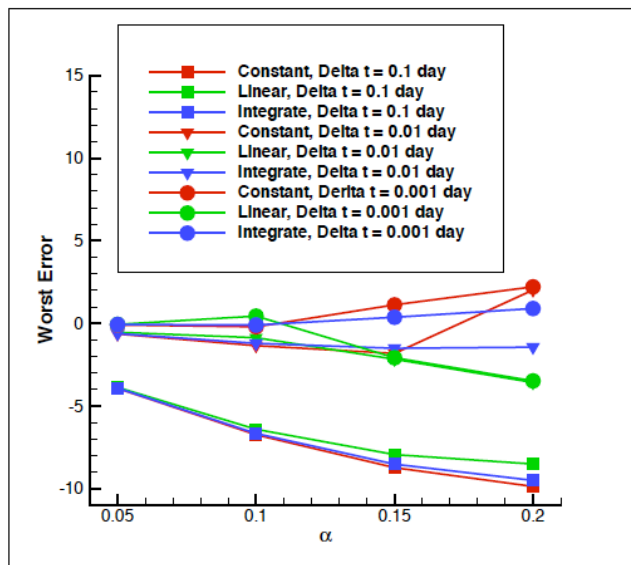


Fig. (7). Plot of worst error (w) of total head (cm) for $\Delta t = 0.1, 0.01,$ and 0.001 day; $L = \alpha = 50$ cm; and $\alpha = 0.05, 0.10, 0.15,$ and 0.2 cm^{-1} after a time period of 0.5 day for the three relative hydraulic conductivity models of constant (C), linear (L), and numerically integrated (I).

However, as α was increased to 0.2 cm^{-1} , the Newton only option became increasingly unstable until it did not work at all. So from the standpoint of robustness of the nonlinear solver, the 20 Picard plus Newton option is the safest choice for the test problem. Other problems such as modeling real-world pump-and-treat remediation systems must be tested before knowing how universal this result is. This is another option for further research.

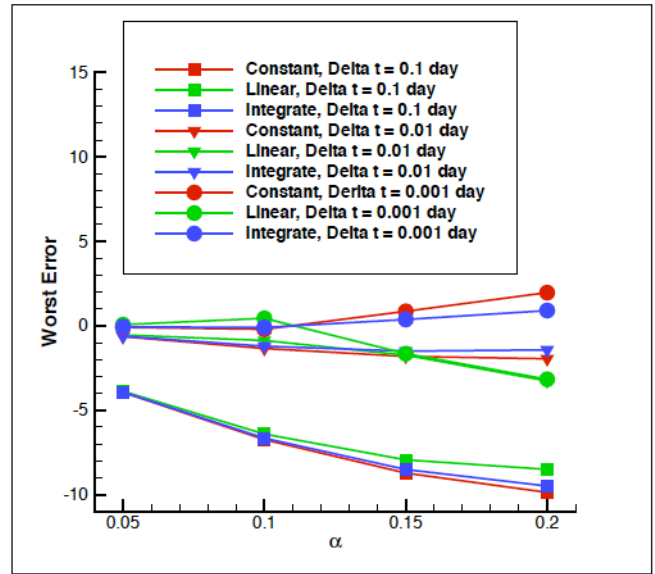


Fig. (8). Plot of worst error (w) of total head (cm) for $\Delta t = 0.1, 0.01,$ and 0.001 day; $L = \alpha = 75$ cm; and $\alpha = 0.05, 0.10, 0.15,$ and 0.2 cm^{-1} after a time period of 0.5 day for the three relative hydraulic conductivity models of constant (C), linear (L), and numerically integrated (I).

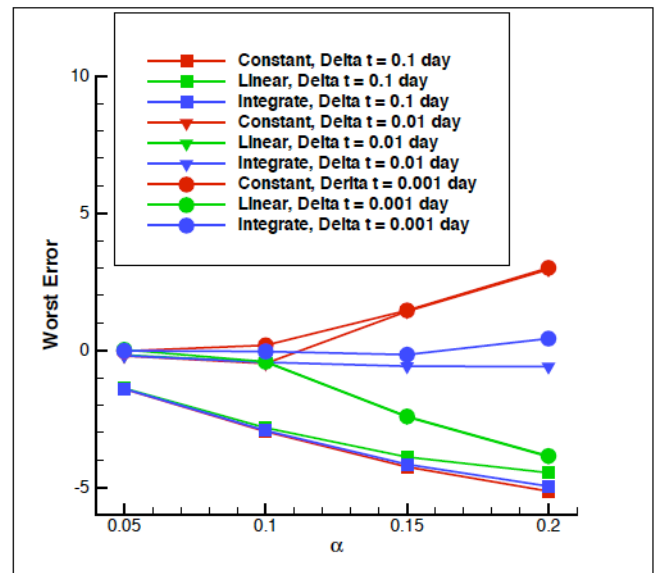


Fig. (9). Plot of worst error (w) of total head (cm) for $\Delta t = 0.1, 0.01,$ and 0.001 day; $L = \alpha = 50$ cm; and $\alpha = 0.05, 0.10, 0.15,$ and 0.2 cm^{-1} after a time period of 2.0 day for the three relative hydraulic conductivity models of constant (C), linear (L), and numerically integrated (I).

7. STEADY-STATE SOLUTION

A steady-state solution can be achieved with either a pseudo-transient time-stepping technique to bring the solution to steady-state by gradually increasing the time-step or by eliminating the time-dependent term up front and solving the remaining steady-state equation. What was done in this study was to use the latter approach, and only the 10 Picard plus Newton nonlinear solver, linear k_r model, 201×201 grid size, and the w metric were used. Fig. 18(c)

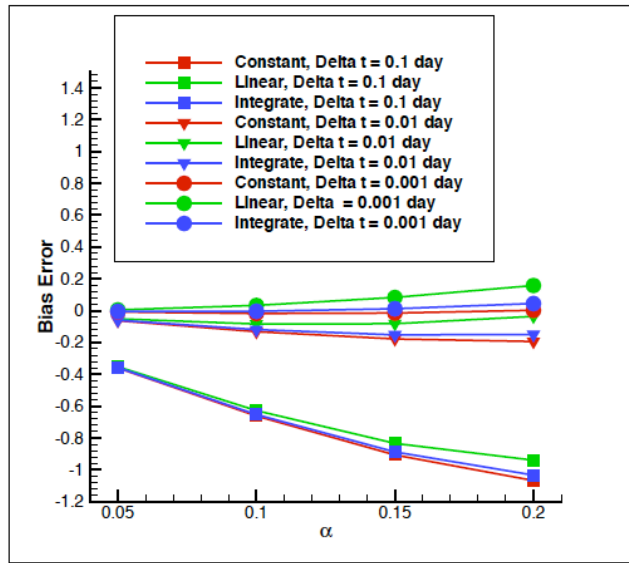


Fig. (10). Plot of bias error (*b*) of total head (cm) for $\Delta t = 0.1, 0.01,$ and 0.001 day; $L = \alpha = 25$ cm; and $\alpha = 0.05, 0.10, 0.15,$ and 0.2 cm^{-1} after a time period of 0.5 day for the three relative hydraulic conductivity models of constant (C), linear (L), and numerically integrated (I).

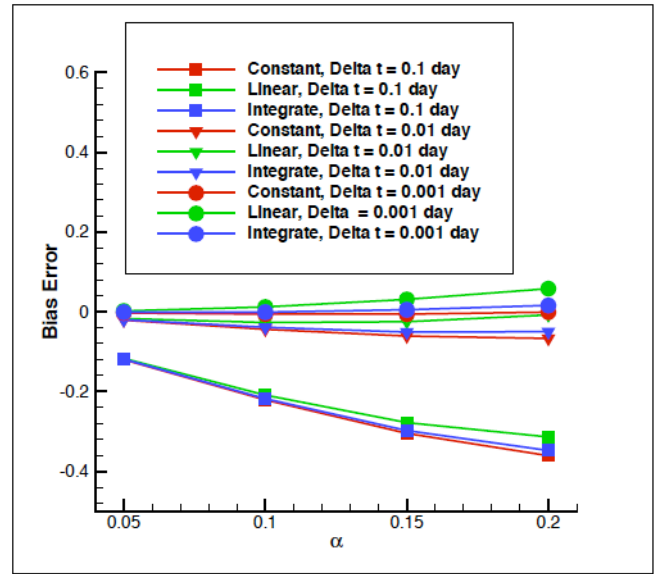


Fig. (12). Plot of bias error (*b*) of total head (cm) for $\Delta t = 0.1, 0.01,$ and 0.001 day; $L = \alpha = 75$ cm; and $\alpha = 0.05, 0.10, 0.15,$ and 0.2 cm^{-1} after a time period of 0.5 day for the three relative hydraulic conductivity models of constant (C), linear (L), and numerically integrated (I).

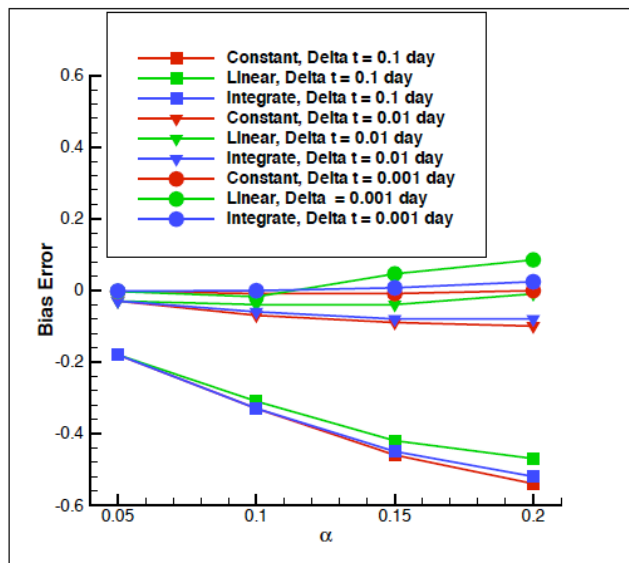


Fig. (11). Plot of bias error (*b*) of total head (cm) for $\Delta t = 0.1, 0.01,$ and 0.001 day; $L = \alpha = 50$ cm; and $\alpha = 0.05, 0.10, 0.15,$ and 0.2 cm^{-1} after a time period of 0.5 day for the three relative hydraulic conductivity models of constant (C), linear (L), and numerically integrated (I).

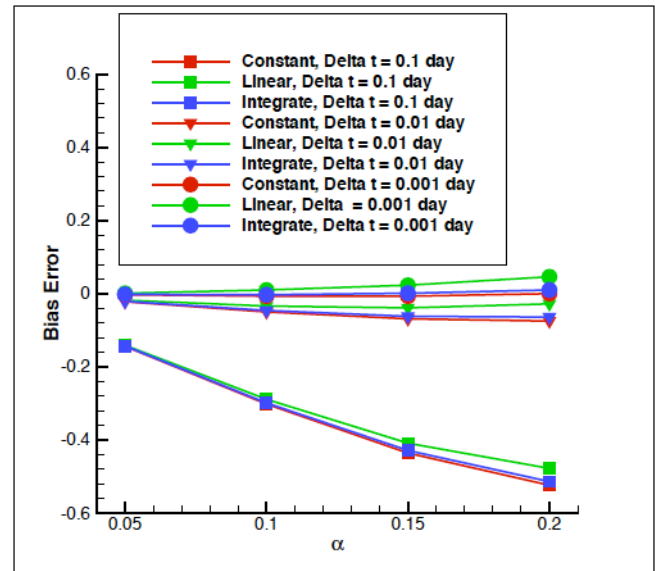


Fig. (13). Plot of bias error (*b*) of total head (cm) for $\Delta t = 0.1, 0.01,$ and 0.001 day; $L = \alpha = 50$ cm; and $\alpha = 0.05, 0.10, 0.15,$ and 0.2 cm^{-1} after a time period of 2.0 day for the three relative hydraulic conductivity models of constant (C), linear (L), and numerically integrated (I).

shows the error (*E*) plot for the steady-state solution at $\alpha = 0.2 \text{ cm}^{-1}$, and Fig. 18(d) shows a zoom of this plot near the bottom of the grid. It is amazing how the error has been shoved so extensively to the bottom of the mesh. This can be explained by observing the total head plot in Fig. 18(a) and zoom of the total head plot in Fig. 18(b). Although the total head ranges from -50 cm to 50 cm, the $\phi = 0$ contour line occurs at less than 10 cm from the bottom at $x = 25$ cm. Thus, the analytical solution drops very sharply in this region, creating a need to refine the grid even more in this

area. Table 2 shows "worst" (*w*) error and position where it occurred for different values of α . As α increases, the errors increase, and the point where they occur is steadily moved toward the bottom.

8. SUMMARY AND CONCLUSIONS

A summary of results of this study are as follows:

1. The simple average relative hydraulic conductivity model inside each finite element performed better than expected.

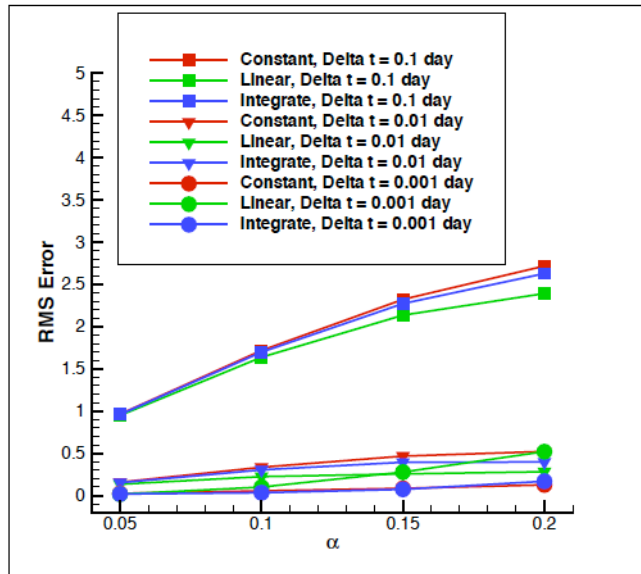


Fig. (14). Plot of RMS error of total head (cm) for $\Delta t = 0.1, 0.01,$ and 0.001 day; $L = \alpha = 25$ cm; and $\alpha = 0.05, 0.10, 0.15,$ and 0.2 cm^{-1} after a time period of 0.5 day for the three relative hydraulic conductivity models of constant (C), linear (L), and numerically integrated (I).

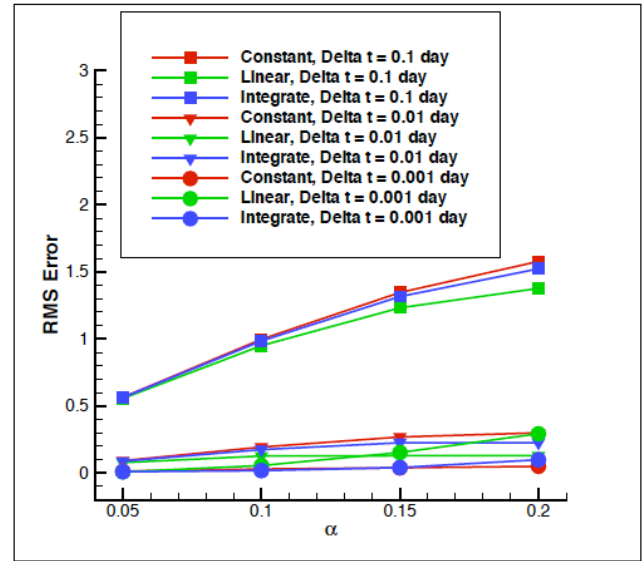


Fig. (16). Plot of RMS error of total head (cm) for $\Delta t = 0.1, 0.01,$ and 0.001 day; $L = \alpha = 75$ cm; and $\alpha = 0.05, 0.10, 0.15,$ and 0.2 cm^{-1} after a time period of 0.5 day for the three relative hydraulic conductivity models of constant (C), linear (L), and numerically integrated (I).

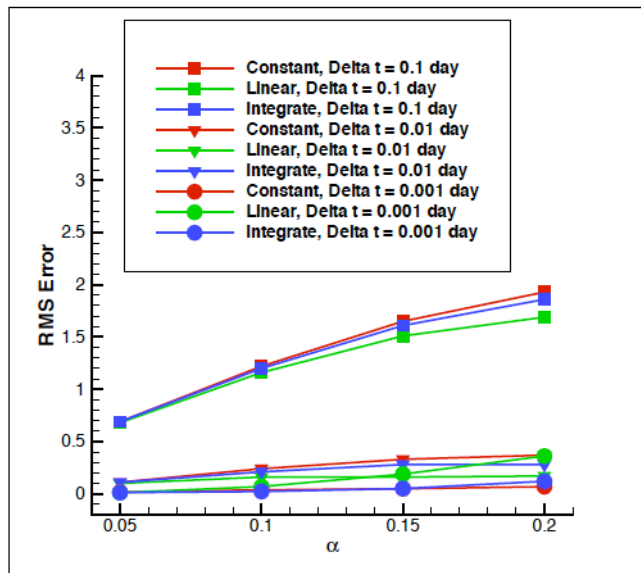


Fig. (15). Plot of RMS error of total head (cm) for $\Delta t = 0.1, 0.01,$ and 0.001 day; $L = \alpha = 50$ cm; and $\alpha = 0.05, 0.10, 0.15,$ and 0.2 cm^{-1} after a time period of 0.5 day for the three relative hydraulic conductivity models of constant (C), linear (L), and numerically integrated (I).

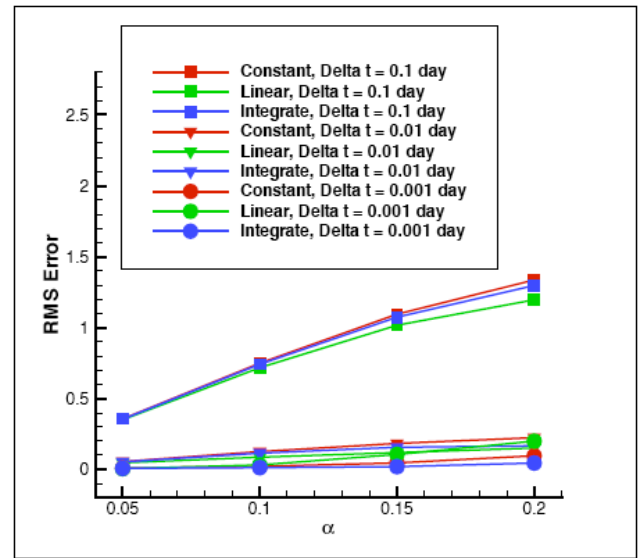


Fig. (17). Plot of RMS error of total head (cm) for $\Delta t = 0.1, 0.01,$ and 0.001 day; $L = \alpha = 50$ cm; and $\alpha = 0.05, 0.10, 0.15,$ and 0.2 cm^{-1} after a time period of 2.0 day for the three relative hydraulic conductivity models of constant (C), linear (L), and numerically integrated (I).

2. The numerically integrated relative hydraulic conductivity model did best as the problem became more nonlinear, especially with difficult boundary conditions at the corners.

3. As α gets larger and the problem becomes more nonlinear, the Newton nonlinear solver struggled to converge.

4. The Picard / Newton solver provided the most stability to the nonlinear solver.

Table 2. Worst Error and Position for The Steady-State Problem for Various Values of α

α	x_{worst}	z_{worst}	Worst Error
0.05	1.25	46.00	-0.006
0.10	0.25	47.75	-0.564
0.15	24.75	0.25	-3.036
0.20	24.50	0.25	-4.824

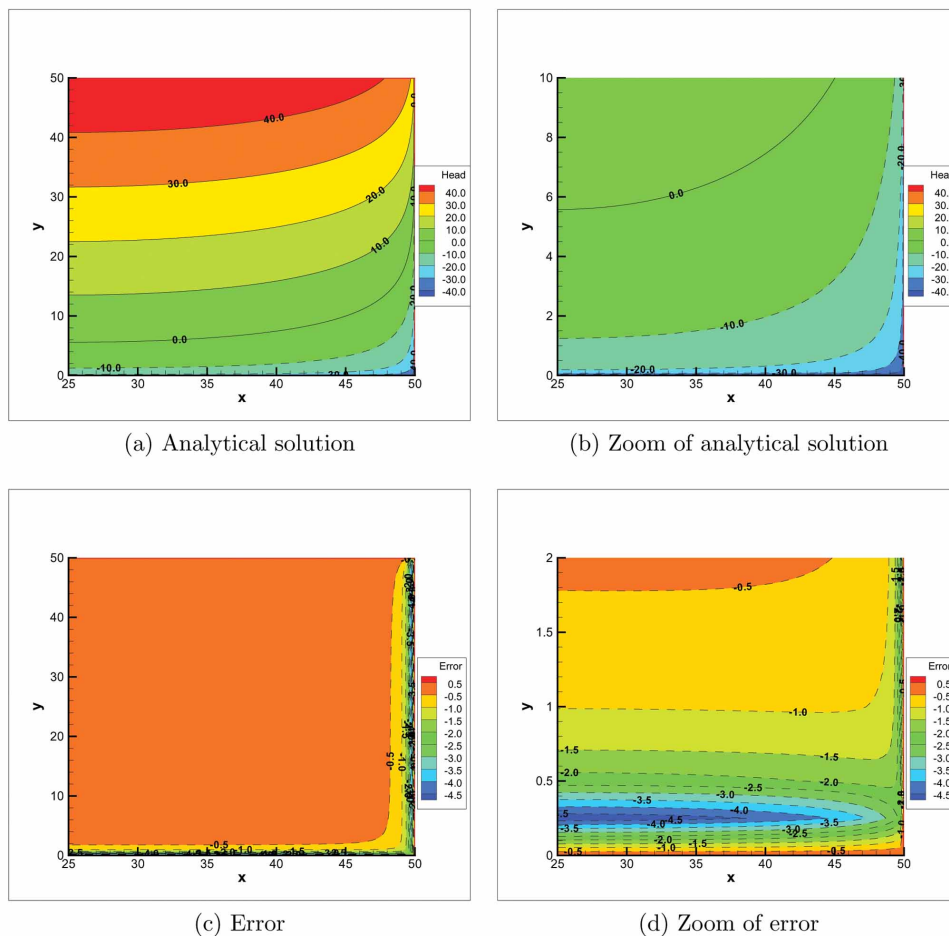


Fig. (18). Plot of the steady-state analytical solution and error in total head (cm) for the right-hand side of the flow region for $\alpha = 0.2 \text{ cm}^{-1}$.

5. Errors are concentrated at the corners for the transient case and the bottom of the mesh for the steady-state case, thus showing a compelling need for adaptive mesh refinement.

6. The more nonlinear the problem is, the smaller the time-step must be.

9. ACKNOWLEDGEMENT

This work was supported in part by a grant of computer time from the DoD High Performance Computing Modernization Program at the ERDC DSRC, Information Technology Laboratory, Vicksburg, MS, USA.

REFERENCES

- [1] Tracy FT. Clean two- and three-dimensional analytical solutions of Richards equation for testing numerical solvers. *Water Resour Res* 2006; 42: W08503.
- [2] Tracy FT. Three-dimensional analytical solutions of Richards' equation for a box-shaped soil sample with piecewise-constant head boundary conditions on the top. *J Hydrol* 2007; 336: 391-400.
- [3] Gardner WR. Some steady-state solutions of the unsaturated moisture flow equation with application to evaporation from a water table. *Soil Sci* 1958; 85 (4): 228-32.
- [4] van Genuchten M. A closed-form equation for producing the hydraulic conductivity of unsaturated soils. *Soil Sci Am J* 1980; 44: 892-8.
- [5] Rucker DF, Warrick AW, Ferré TPA. Parameter equivalence for the Gardner and van Genuchten soil hydraulic conductivity functions for steady vertical flow with inclusions. *Adv Water Res* 2005; 28: 689-99.
- [6] Irmay S. On the hydraulic conductivity of unsaturated soils. *Econ Transit, AGU* 1954; 35.
- [7] Istok J. Groundwater modeling by the finite element method. *AGU* 1989.
- [8] Kelley CT. Solving nonlinear equations with Newton's method. *USA, SIAM* 2003, 104.
- [9] Cook RD. Concepts and applications of finite element analysis. 2nd ed. New York; John Wiley & Sons 1981.
- [10] Putti M, and Paniconi C. Evaluation of the Picard and Newton iteration schemes for three-dimensional unsaturated flow. *Proceedings of the 9th International Conference on Computational Methods in Water Resources, Denver, CO, USA, Jun 1992.*

Received: November 19, 2008

Revised: July 19, 2010

Accepted: August 07, 2010

© F.T. Tracy; Licensee Bentham Open.

This is an open access article licensed under the terms of the Creative Commons Attribution Non-Commercial License (<http://creativecommons.org/licenses/by-nc/3.0/>) which permits unrestricted, non-commercial use, distribution and reproduction in any medium, provided the work is properly cited.